Frontiers in Mechanochemistry and Mechanical Alloying

INCOME2008
1-4 December, 2008

ULTRAFINE GRAINED MATERIALS THROUGH MECHANICAL PROCESSING: AN ASSESSMENT

K.A. Padmanabhan[1,2ξ], S. Balasivanandha Prabu[2]
[1]Institute of Materials Physics, University of Muenster, D 48149 Muenster, Germany
[2]Materials Science and Engineering Division, Department of Mechanical Engineering, Anna University, Chennai 600 025, India

Keywords: Severe Plastic Deformation (SPD), Ultrafine Grained Materials, Friction Stir Processing

Abstract

In this paper severe plastic deformation (SPD) and friction stir processing/ welding are examined. The structural changes due to SPD are reflected in improved mechanical properties. Advantages of SPD are pointed out. Within the SPD technique, a number of approaches are possible, e.g., equi-channel angular pressing/ extrusion, high pressure torsion, accumulative roll bonding/fold - roll process, reciprocating extrusion – compression, cyclic close die forging, repetitive corrugation and straightening. Analyses available are elementary and often assume uniform stress and strain distribution. These processes are easily adapted to suit standard metal working equipment fitted with inexpensive devices and tools. However, scaling up the processes to handle large billets and achieve large tonnage production is difficult. In the near future, medium and small-scale industrial production only is likely.

Friction stir process, a solid state technique for joining similar or dissimilar materials of equal or different thickness, has some key metallurgical, environmental and energy benefits. It is already being considered for applications in aerospace and automotive industries. Significant improvements in surface properties and superplastic flow have been established in friction stir processed materials. Velocity of tool movement and power input needed for fast rotation of the tool are the major variables. Since significant temperature rise is there during processing, in a proper analysis, the boundary conditions arising from thermal and mechanical constraints have to be satisfied simultaneously, which is an extremely difficult. A few key issues have to be addressed before large-scale production can be attempted. An integral approach that takes into account the total system of material, design, mechanics and component forming is likely to lead to industrially relevant solutions.

Introduction

Synthesizing massive nanostructured materials, with a grain size considerably smaller than 100 nm, presents a challenge to basic research as well as to application-related processing efforts. Production of ultrafine-grained (UFG) microstructures in metals and alloys having different crystal structures, but always an initially coarse microstructure, using severe plastic deformation (SPD) can significantly enhance the physical and mechanical properties of materials. SPD leads to the formation of sub-micrometer and nano-grained structures that could display high strength and significant ductility at room temperature. For defining a submicron grain structure the important parameters are average spacing between high angle grain boundaries (HAGB) and the proportion of HAGB area to the total area. The reported effects on properties include increased hardness and yield stress, both having a tendency to saturation for given experimental conditions. The drawback sometimes is limited ductility. SPD procedures are attractive because they lead to very significant grain refinement to the submicrometer or even nanometer level [1,2].

Some well-known SPD techniques are: equal channel angular pressing (ECAP [3]); high pressure torsion (HPT [4]); accumulative roll bonding (ARB [5]); reciprocating extrusion-compression (REC [6]); cyclic close die forging (CCDF [7]); repetitive corrugation and straightening (RCS [8]).

In contrast to traditional cold rolling or drawing processes, SPD techniques often use strongly non-proportional strain paths. In a number of papers the resulting microstructure and superior mechanical properties (e.g., extreme strength) have been investigated experimentally. For instance, the subgrain size, misorientation angle across boundaries, the fraction of high-angle grain boundary (HAGB) area and flow stress or microhardness have been measured as a function of the accumulated plastic strain for cyclic SPD and rolling [8].

Equal Channel Angular Pressing

Severe plastic deformation by equal-channel angular pressing (ECAP) has received much attention in recent years and is the most frequently used SPD process. Invented by Segal in Russia in 1977, ECAP is based on simple shear taking place in a thin layer at the crossing plane of the equal channels. This leads to a low force requirement (small presses can be used) and the resulting tool pressure is also low. This, together with the simple tool geometry, makes laboratory tooling easily attainable. In many laboratories the researchers have found the ECAP method a convenient tool for investigating the relationship between the applied strain and the structure developed [2]. Processing by ECAP has been used effectively with a very wide range of in face-centered cubic (fcc) metals, but the application of ECAP to hexagonal close-packed (hcp) metals is more difficult because of the limited number of active slip systems [9]. Much of the work has been carried out on single-phase materials, with a major effort concentrated on Al alloys, where grain sizes below 200 nm have

Present address : School of Engineering Sciences & Technology
Central University of Hyderabad, Hyderabad 500 046, India
ξ email: ananthaster@gmail.com

been obtained. It has been shown that sub-micrometer scale equiaxed or nearly equiaxed grains with high-angle grain boundaries can be produced by ECAP in face-centered cubic (fcc), body-centered cubic (bcc) and hexagonal close packed (hcp) metals [10,11].

Principles of Processing by ECAP

It is relatively easy to set up and use an ECAP die, where exceptionally high strains may be imposed through repetitive pressing. It has been suggested that the ECAP samples can be easily scaled-up to produce relatively large bulk materials and that it can be incorporated into conventional rolling mills for use in continuous processing or into the ECAP-conform process for the production of wires [12]. A counter-view that scale-up and ensuring a high rate of production required by industry is extremely difficult (as ECAP is a batch process) is also available. In that view only medium and small-scale production requirements can be met by this technique at least in the fore-seeable future [13]. Figure 1 shows the process of ECAP and different geometry of the process.

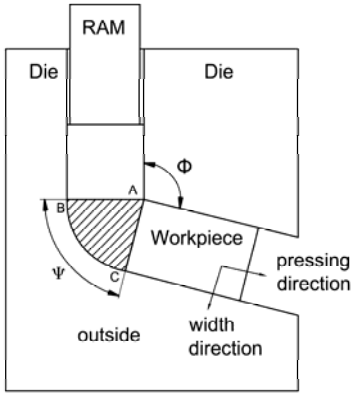

Figure1. Schematic illustration of the ECAP process showing the die channel angle geometry. Pressing direction, width direction and thickness direction denote three perpendicular directions with reference to the work piece [14].

The strain imposed on the sample in each passage through the die is dependent primarily upon the angle, Φ, between the two parts of the channel (90° in Fig. 2(a)) and also to an insignificant extent upon the angle of curvature, Ψ, representing the outer arc of curvature where the two channels intersect [12].

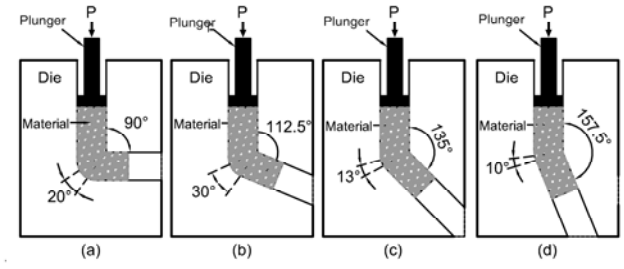

Figure 2. Schematic illustration of the dies used to evaluate the influence of the channel angle, ϕ: the values of ϕ are (a) 90°, (b) 112.5°, (c) 135° and (d) 157.5° [15]

ECAP processing at a high temperature will improve the workability of materials. But, ECAP processing to very high strains at high temperatures leads to a coarser grain structure than what is produced at room temperature with lower imposed strains. Although the total strain imposed at high temperatures can be very large, the simultaneous activation of recovery processes means that retained dislocation and boundary densities are much lower than for room temperature deformation. The net result is a somewhat coarser final microstructure [16].

The ECAP parameters, viz., amount of deformation, shear strain (e), number of passes (N), rotation angle between each repetitive pressing, the strain rate monitored by movement of punch, and the temperature during processing greatly influence the final microstructure.

The shear strain value depends strongly on the number of passes (N) and the curvature angle at the channel intersection and can be generalized as follows:

$$\varepsilon = \frac{N}{\sqrt{3}}\left[2\cot\left(\frac{\phi}{2}+\frac{\psi}{2}\right)+\phi\cos ec\left(\frac{\phi}{2}+\frac{\psi}{2}\right)\right] \quad (1)$$

The strain rate in ECAP depends on the diameter (for round cross-section) or width (for square cross-section) of the billet and the ram speed.

According to Eq. (1), the equivalent strain,ε, decreases with the corner angle ψ, as shown in Fig. 3 (a) and (b).

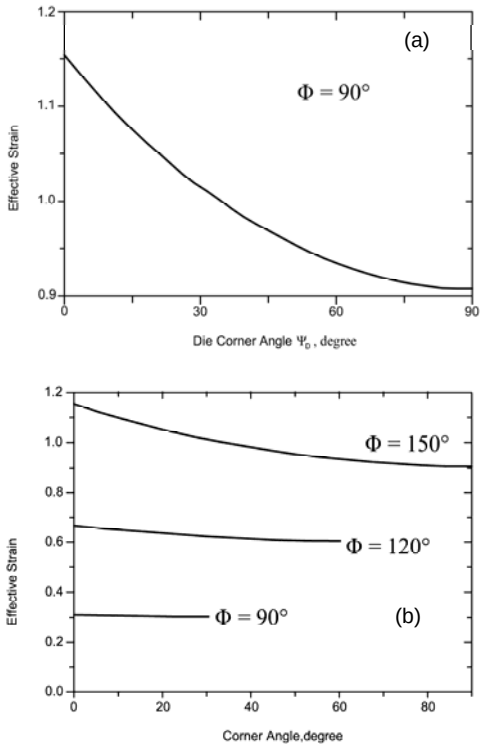

Figure 3. Results obtained in a very elementary analysis which assumes uniform deformation [17]

It can be seen in Fig. 3 that the effective strain during ECAP can decrease from a maximum of 1.15 to a minimum of 0.907, when the corner angle increases from 0° to 90°, with the channel angle fixed at ϕ=90°. It should, however, be noted that the effect of the corner angle is already included in the equation used for predicting the strain.

Figure 4 shows the evolution of the equivalent plastic strain for a die with L_0=10 mm and R =10 mm where angle, ψ, as defined, can be determined from Eq. (2) [18].

$$\tan\left(\frac{\psi}{2}\right) = \frac{0.5R\sin(\phi)}{L_0 - R\cos^2\left(\frac{\phi}{2}\right)} \quad (2)$$

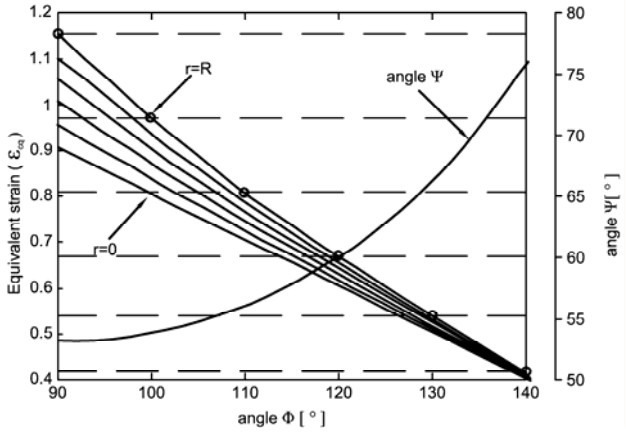

Figure 4. Equivalent plastic strain for different die geometry and ψ angle for L_0 = 10 mm and R = 10 mm, where L_0= Diameter of the die; R is the outer fillet radius; Ψ – Die corner angle [18]

Other factors which influence ECAP processing may also strongly affect the deformed microstructure. Examples are the processing route, the die angle between the inlet and outlet channels (die channel angle) and the strain rate. The influence of some of these parameters has been studied extensively on aluminium alloys whereas others alloys have received less attention. Only a few reports are available on the effect of channel angle on the grain refinement process in aluminium alloys and these studies are not able to account for the changes occurring as a result of deformation completely [19].

It is generally found that the minimum grain size that can be obtained by severe deformation is of the order of the subgrain size. The finest grain size that can be achieved, therefore, decreases at lower homologous processing temperatures (Fig. 5) and at higher strain rates. The grain size is also finer in low stacking fault energy (SFE), planar-glide materials and in alloys that contain elements that have a strong effect on inhibiting recovery, e.g., Mg in Al. From Figure 5 it can be seen that sub-micrometer grain structures can be produced by severe deformation processing at temperatures of <0.4*T*m, while nanocrystalline structures can only be produced below 0.2*T*m. Unfortunately, most alloys cannot be processed below 0.2*T*m without fracture, except by using techniques like SPTS, which are carried out under large hydrostatic pressures [20].

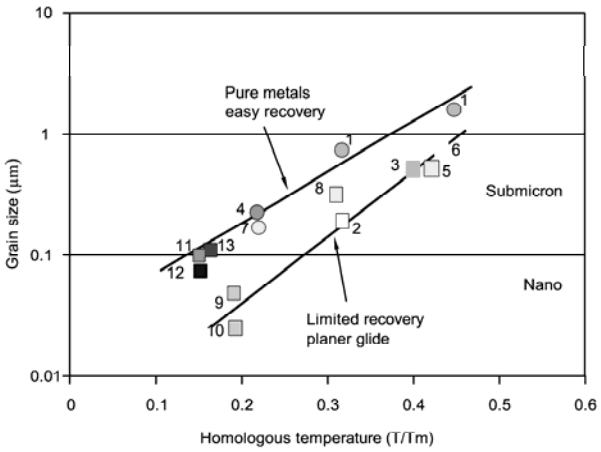

Figure 5. Grain sizes measured in severely deformed alloys processed by ECAE, ARB and severe plastic torsion straining (SPTS), plotted against homologous temperature: ECAE: (1) Al; (2) Al–3%Mg; (3) IF steel; (4) Cu; (5) ARB: IF steel; SPTS: (6) Zn–22Al; (7) Cu; (8) Mg; (9) and (10) $AlNi_3$; (11) Fe; (12) Ti; and (13) Ni. The data are grouped between upper and lower bounds that represent materials with high SFE that recover relatively easily and materials with low SFE that exhibit planar glide and more limited recovery [20]

To sum up, equal channel angular extrusion is a unique process for the following reasons.

1. Relatively uniform structure and properties are developed throughout the worked materials. But, at local levels there are significant variations [21].
2. A large equivalent deformation per pass and an extremely large total effective deformation after multiple passing occur without any appreciable change of the initial billet cross-section.
3. Relatively low pressures and loads are sufficient for extrusion. (The magnitude, however, will depend on the material and billet size.)
4. The creation of special structures and textures are possible because of reasonably strict control over the direction of shear, the homogeneous stress-strain state, the capacity for extremely large deformation, in principle, in massive products and the opportunity to modify the shear plane and direction during a multiple extrusion sequence. (But, the specimen cross-section cannot be changed by processing and when the size of the billet is large, constructing containers of sufficient strength that could hold the billets without breaking could constitute some design and materials selection problems.)
5. The stimulation of specific mechanisms of microstructure formation and phase transformation are possible.
6. The process is not difficult to realize via standard metal-working equipment fitted with inexpensive devices and tools.

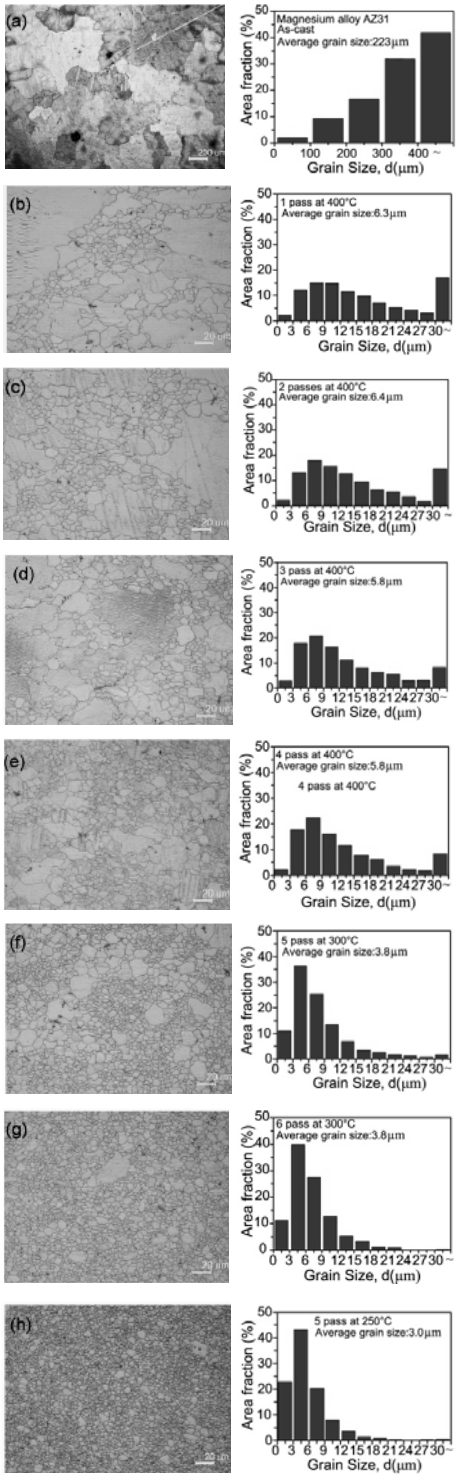

Figure 6. Optical micrographs showing the microstructural changes and grain size distributions for different ECAP conditions: (a) as-received, (b) Case A (400°C/1 passes ECAP), (c) Case B (400°C/2 passes ECAP), (d) Case C (400°C/3 passes ECAP), (e) Case D (400°C/4 passes ECAP), (f) Case E (300°C/5 passes ECAP), (g) Case F (300°C/6 passes ECAP) , (h) Case G (250°C/5 passes ECAP). Magnesium alloy AZ31 [22]

Grain Refinement

The effect of processing conditions like the number of passes and temperature on grain refinement during ECAP experiments was investigated by Kang *et al,* 2008 [22].

During plastic deformation at temperatures <0.4*T*m, new HAGB areas are generated by two mechanisms that operate simultaneously: (i) extension of pre-existing boundaries in proportion to the strain, and (ii) the formation of new HAGBs by grain subdivision [20]. Figure 6 displays optical micrographs which illustrate the grain refinement and grain size distribution processes during multi-pass ECAP. As can be seen from these pictures, the microstructure of the as cast ECAP billet with a grain size of 223 μm got refined to about 3 μm after 5 passess at 250°C. This was due to accumulated shear strain and dynamic recrystallization. The processing temperature has an important role in grain refinement. In fact, both dynamic recrystallization and grain growth take place during ECAP at relatively high temperatures (above about 250°C for this Mg alloy) and the resultant grain size is bigger than that at a lower temperature.

Figure 7 shows the changes in grain size and microhardness with the processing temperature. As can be seen, the grain size and microhardness remained nearly constant up to 350°C. From this finding a processing temperature of 300°C was chosen and the punch speed was 0.2 m/s (equal to a strain rate of about 0.0017 s^{-1}) [22]. On close examination, it could be established that both the microstructure and microhardness varied as one went from the specimen periphery to the centre (Fig. 8).

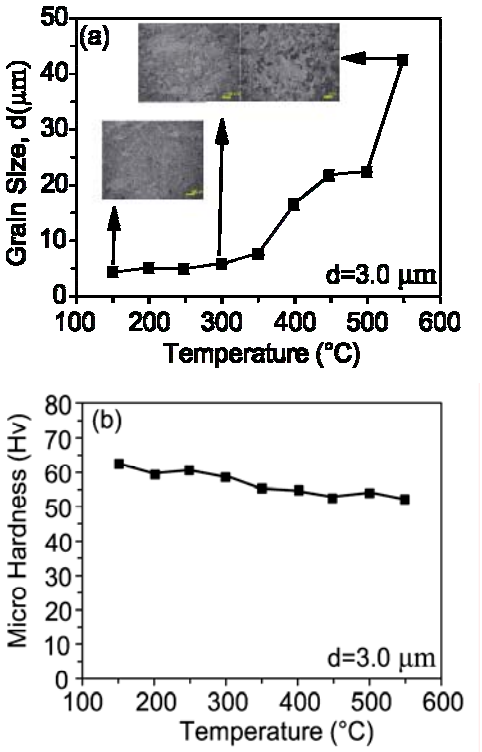

Figure 7. Changes in the (a) grain size, and (b) microhardness at various temperatures. Initial grain size is indicated at right hand bottom corner [22]

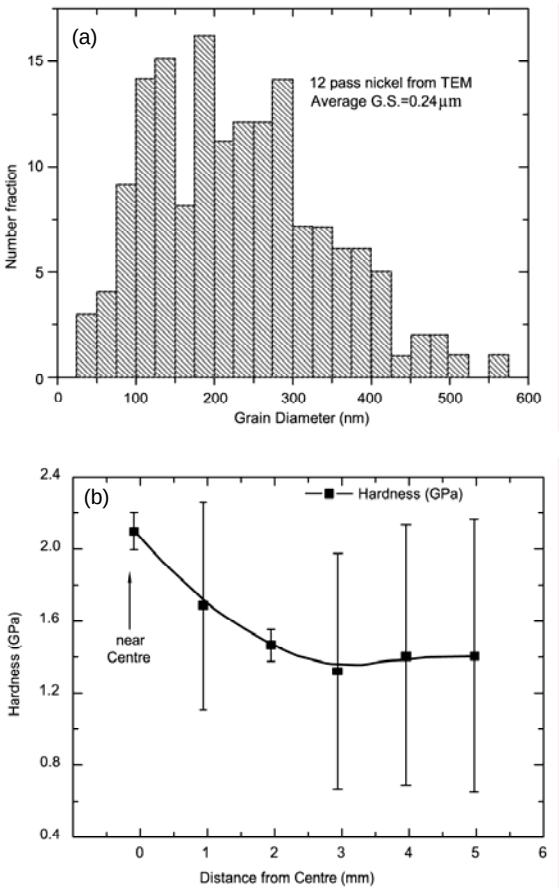

Figure 8. (a) Grain size distribution plot of nickel processed through ECAP deformed to a strain ~12 at room temperature. (b) Measurement of Vickers micro-hardness from the centre to the periphery of the sample for a load of 25 g for 45 s [21]

High Pressure Torsion

The principle of processing by HPT is based on the classic work of Bridgman in which thin discs were subjected to compression and torsion to produce large strains [23]. Torsional straining is inhomogeneous across the diameter of the sample. However, there are reports of production of reasonably homogeneous microstructures in an aluminum-based alloy, pure copper and pure nickel, as well as in titanium and nickel-aluminide [23].

Two important experimental parameters that define HPT processing are: the imposed pressure, P, and the total strain, ε [23]. A schematic representation of the process is given in Fig. 9.

Processing by high-pressure torsion produces a situation where, in principle at least, there is zero strain at the center of the disk and the strain increases towards the periphery [27]. This is opposite of what is seen during ECAP (see Fig. 8)

Obviously, plots like Fig. 8 and Fig. 10 cannot result if the stress and strain are uniform throughout the sample, as assumed while determining the effective strain per pass/ revolution etc. Visioplasticity, coupled with finite element analysis, may lead to a more realistic description.

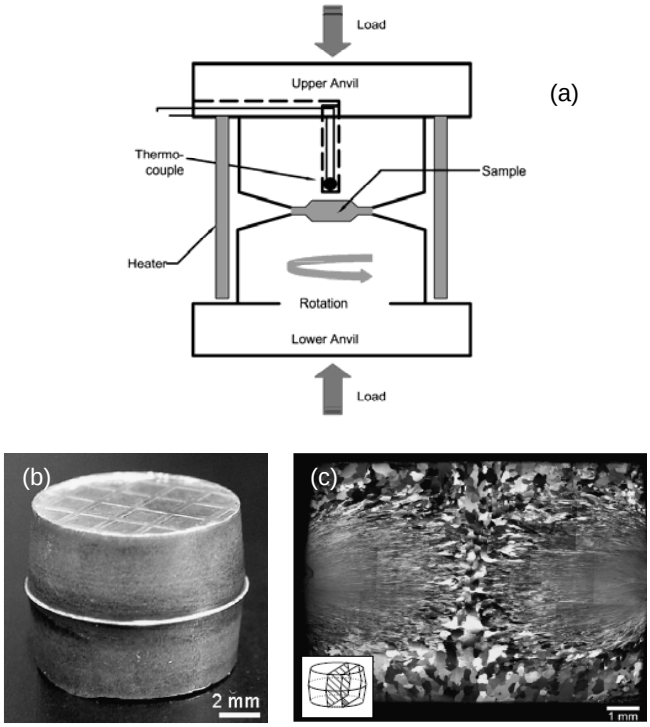

Figure 9. (a) Schematic illustration of the HPT set up [25]. (b) Appearance of a bulk sample after HPT through a single turn. (c) Montage of microstructures after two turns: the plane of sectioning is shown at the lower left (b), (c) [26])

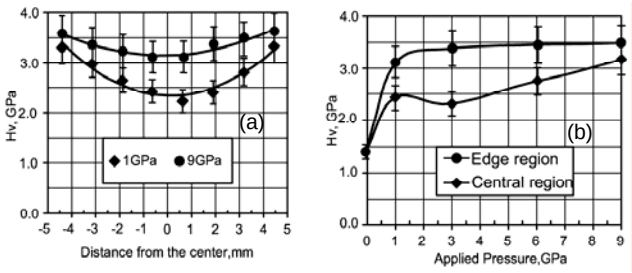

Figure 10. Microhardness profile of HPT processed nickel at two different applied pressures (a); average microhardness for the central and edge regions as a function of applied pressure for HPT nickel (b). Samples were subjected to HPT pressing at room temperature through 5 whole turns [28]

In contrast, often grain sizes and shapes do not change, while the density of lattice defects and strength of the material decrease due to recovery, when materials are subjected to ordinary plastic deformation.

Three obvious questions [29] that arise from the studies completed so far are:

1. How does one crystal get fragmented into many volume elements of widely differing orientations?
2. What is the microstructure after the fragmentation?
3. How can a steady-state be reached with increasing strain in such non-steady state processes?

Friction Stir Processing

Friction stir processing (FSP) is an important grain refining technique. FSP is the generic name for processes based on the friction stirring principle used in the parent process, viz., friction stir welding (FSW). Recently, FSP has drawn much attention as a tool for producing superplastic aluminum alloys due to its capacity to result in very fine grain sizes and high grain boundary misorientations in friction stir processed microstructures. However, the extent of superplasticity in FSP aluminum alloys, despite favorable microstructural characteristics, becomes limited due to the evolution of unstable microstructures at elevated temperatures [30].

An essential strategy for reducing the weight of automobiles consists of increasing the use of lightweight materials, such as aluminium or metal composites that combine metals with other materials. However, difficulties associated with welding these materials have limited their use in many automotive components. In traditional welding processes melting can destroy the carefully engineered microstructures of composites thereby eliminating their unique properties. Even in aluminium sheets or castings, a number of significant issues arise from welding. For example, undesirable chemical interactions can occur between aluminium and the welding equipment when aluminium sheets are resistance spot welded. This can contribute to weak welds and can also accelerate the deterioration of the welding equipment. Welds made in aluminium castings can contain porosity. They can also be susceptible to cracking associated with the metallurgical changes that occur during localized melting. Many of these problems are eliminated in Friction Stir Welding, a solid state welding process (Fig. 11).

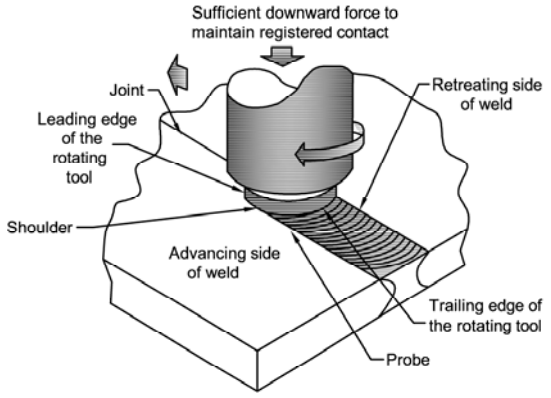

Figure 11. Friction stir processing (FSP), a solid-state technique for joining materials and a tool for material processing (*i.e*., surface machining) [31]

FSW has been used successfully in many joining applications. A rotating tool plunges into a part where the material plastically deforms due to an elevated temperature field produced by adiabatic heating. The tool traverses along, or across, the intersection of two parts, joining the parts as the tool leaves the processing zone and deformed material fills the void left by the tool. The FSW process has advantages in that it can weld materials that are difficult to weld using conventional processes (e.g., 2XXX and 7XXX aluminium alloys) and is environmentally friendly since harmful gases (or gases that contribute to global warming) are not required during the operation. A schematic representation of the friction stir butt welding process is shown in Fig. 11.

The tool consists of a pin and shoulder, both of which contact the part material, and slowly plunges into one sheet where it dwells for a specified amount of time. Once the processing zone consists of plastically deformed material at an elevated temperature, the tool moves towards the other sheet, usually at a constant velocity. When the tool travels from the first sheet to the second a weld is formed between the two sheets. While most welds are along the interface between the two sheets, some welds are in the transverse direction.

During FSW, heat is generated by the friction between the tool and the workpiece and by the plastic deformation occurring around the tool. Understanding the temperature distribution is necessary, as it influences the weld microstructure and the resulting mechanical properties.

The main features of friction stirred components (FSC) are as follows:

1. The profiled tool is rotated such that the material flow is upwards towards the tool shoulder.
2. An initial clearance is provided between the shoulder and the workpiece, where the material from the base of the pin is deposited.
3. This distance between the tool shoulder and the workpiece can be adjusted to control the shape, size, and integrity of the channel.

Material in contact with the pin is expected to rotate with the velocity of the tool. However, there is evidence that in some cases a slipping or sticking/ slipping boundary condition prevails.

A summary of the key issues that are to be considered while setting up the constitutive equations and the boundary value problem for this technique are presented in Fig. 12. The key benefits of FSW are summarized in Table 1.

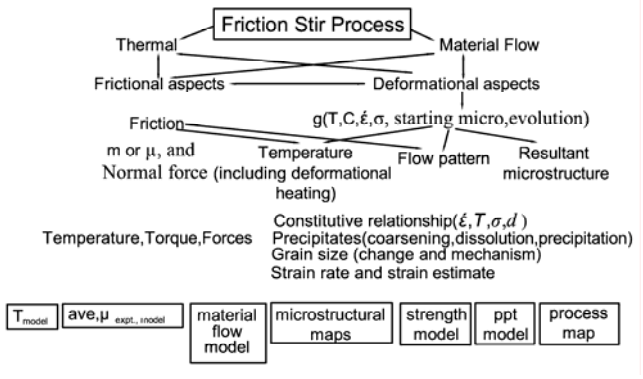

Figure 12. A summary of various aspects of the friction stir process needed for constitutive modeling [32]

Table 1. Key benefits of friction stir welding

Metallurgical benefits	Environmental benefits	Energy benefits
Solid phase process Low distortion of workpiece Good dimensional stability and repeatability No loss of alloying elements Improved microstructures and surface properties Excellent metallurgical properties in the joint area Absence of cracking Replace multiple parts joined by fasteners Can join similar and dissimilar materials which cannot be joined otherwise.	No shielding gas required No surface cleaning required Eliminates grinding wastes Eliminates solvents required for degreasing Consumable materials saving such as rugs, wire or any other gases.	Improved materials use (e.g., joining different thicknesses); allows reduction in weight; only 2.5% of the energy needed for a laser weld. Decreased fuel consumption in light weight aircraft, automotive and ship applications.

Figure 13(a) and 13(b) show the tested specimens of the FSP Al-4Mg-1Zr alloy deformed to failure at 525°C at different strain rates and at different temperatures for a strain rate of $1X10^{-1}$ s^{-1}. The specimens show neck-free elongation, which is a characteristic of superplastic flow. It was revealed that a considerable amount of material flow from the grip region into the gage section occurred during the tensile tests in ECAP Al-5.5Mg-2.2Li-0.12Zr, ECAP Al-3Mg-0.2Sc, and 5083Al (again a well-known characteristic of superplastic deformation). This alters the deformation conditions continuously and by supplying more material than what would be the case if the deformation were to take place at constant volume, result in an over-estimation of the degree of superplasticity. This effect is minimized with the use of longer gage length specimens.

Influence of Processing Parameters

The FSW/ FSP process involves complex material movement and plastic deformation. Welding parameters, tool geometry and joint design exert a significant effect on the material flow pattern and temperature distribution, thereby influencing microstructure evolution. In this section, a few major factors affecting the FSW/ FSP process, such as tool geometry, welding parameters and joint design are considered. The influence of the processing parameters is intriguing and has not been understood fully. Due to the

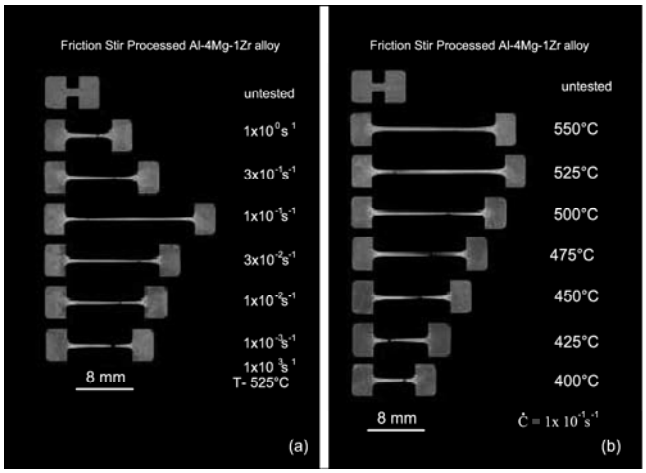

Figure 13. Appearance of specimens before and after superplastic deformation at (a) 525°C and different strain rates, and (b) $1x10^{-1}$ s^{-1} and different temperatures [33]

knowledge of microstructural evolution as a function of processing parameters being limited, its influence on abnormal grain growth (AGG) behavior is also not well understood**.**

The factors that can affect the onset of AGG are: (i) anisotropy in grain boundary energy and mobility; (ii) reduction in pinning forces due to coarsening and/ or dissolution of particles; and (iii) thermodynamic driving forces due to grain size distribution. An analysis available in the literature notes that AGG becomes possible when the pinning parameter ($Z = 3\ FvR/d$, where Fv is the volume fraction of particles, R is the average grain radius and d is the average particle diameter) is in the range $0.25<Z< 1$. From this it is clear that the presence of a high volume fraction of fine, thermally stable dispersoids may help control the AGG behavior, regardless of the other microstructural characteristics. Indeed, FSP Al–4Mg–1Zr alloy did not show any sign of AGG even at rather high temperatures because of the presence of a high volume fraction of fine Al_3Zr particles.

The experimental data are plotted on the microstructural stability map (Fig. 14). It shows that the combination of the pinning parameter and grain size ratio (= largest grain size/average grain size) just falls within the AGG regime [30].

Figure 15 shows the variation of flow stress with initial strain rate and temperature for both FSP and cast A356 alloy. The maximum strain rate sensitivity of 0.45 at an initial strain rate of 1×10^{-3} s^{-1} corresponds to a maximum elongation of 650%. Based on the value of the strain rate sensitivity index, grain boundary sliding is suggested to be the dominant deformation mechanism [25]. Furthermore, flow stress of the FSP sample is significantly lower than that of the cast specimen at an initial strain rate $<3 \times 10^{-2}$ s^{-1} at 530°C and at temperatures in the range of 470–570°C at an initial strain rate of $1x10^{-3}$ s^{-1}. This is traced to a significantly refined microstructure in the FSP sample [35].

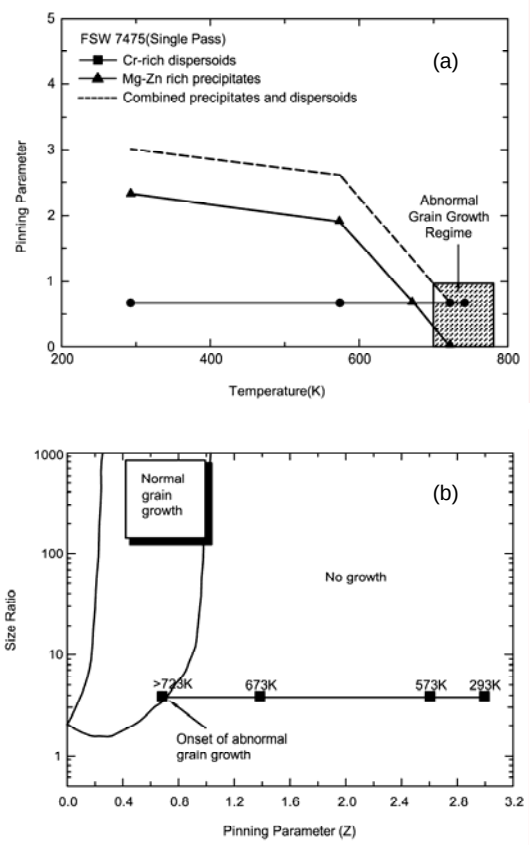

Figure 14. (a) Pinning parameter vs. temperature and (b) microstructural stability map for FSW 7475 Al [34]

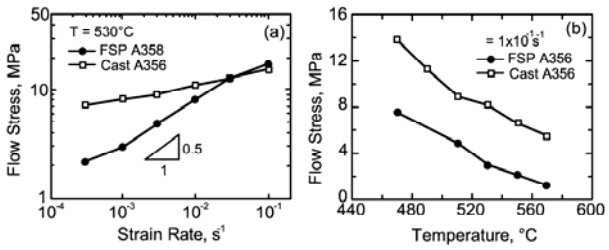

Figure 15. Variation of flow stress with (a) initial strain rate, and (b) temperature for both FSP and cast A356 [35]

The visual aspect of the welds, characterized by limited flash and tunnelling phenomena was improved with increasing values of the applied load (F), weld speed (V) and rotation rate (W). The AZ31 friction stir welded microstructure consists of three different zones: the nugget, the TMAZ and the HAZ/ base metal (as no difference in grain size between the HAZ and the base metal could be observed). When studying the influence of the welding parameters on the grain size, several conclusions could be drawn. First, it appears that a large microstructure gradient is present in the TMAZ at low (W, V) values, whereas this gradient is smaller at high (W, V) values (Fig. 16). (In this figure, W corresponds to the tool rotation speed and V to the welding speed.) Moreover, in the weld nugget, relatively small grains are observed at low (V, W). Increasing W leads to an increase in grain size and in grain size dispersion. Increasing V causes a decrease in grain size. At high W, there is no longer any influence of the welding speed on the grain size. Increasing the shoulder diameter leads to an increase in grain size (Fig. 17). This is mainly due to the relationship between the welding parameters and the adiabatic temperature rise during FSW. Indeed, increasing the shoulder diameter and the tool rotation speed (W) or decreasing the welding speed (V) increases the heat generated during the process and promotes grain growth.

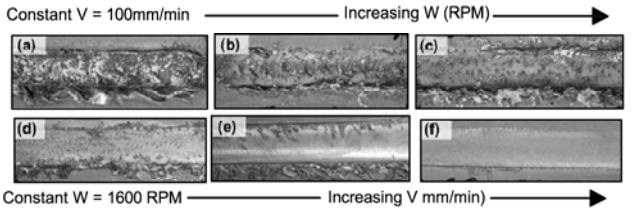

Figure 16. Digital images of the superficial aspect of several ‘‘bead on plate” AZ31 welds: (a) W = 400 rpm, V = 100 mm min^{-1} (b) W = 700 rpm, V = 100 mm min^{-1}; (c) W = 900 rpm, V = 100 mm min^{-1}; (d) W = 1600 rpm, V = 400 mm min^{-1}; (e) W = 1600 rpm, V = 600 mm min^{-1}; (f) W = 1600 rpm, V = 1000 mm min^{-1} [36]

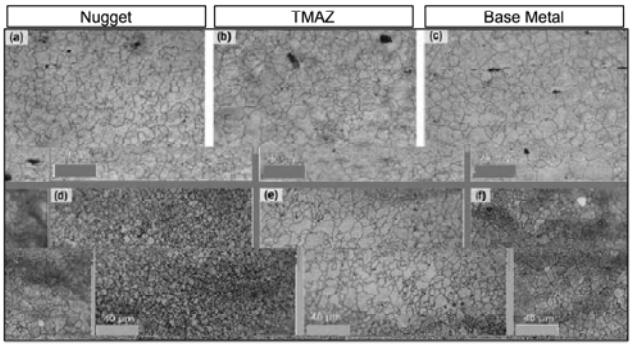

Figure 17. Grain size evolution with shoulder diameter for 1000 rpm, 200 mm min^{-1} butt FSW: (a)–(c) 13 mm shoulder diameter; (d)–(f) 10 mm shoulder diameter [36]. TMAZ - Thermomechanically affected zone

Figure 18 shows the grain structure of the as-received material and FS processed samples at 1200 rpm rotational speed and 22 and 25 in. / min translational speeds, respectively. The as-received material has a fine microstructure with an average grain size of about 6 μm. It is observed that although there is not much grain refinement after FSP, the grain structure is clearly more equiaxed and more homogenized. It is clearly demonstrated that FSP refined the microstructure from an average grain size of about 6 μm to an average grain size of about 3–4μm. More importantly, the distribution of grain size is clearly shifted and concentrated to the left, which indicates more refinement and a more homogenous equiaxed structure. The as-received structure consists of a combination of large and small grains, while the structure of the processed samples shows that the majority of grains have almost the same grain size. The finer and more homogenous grain structure produced by FSP is expected to improve the ductility and formability of the material at elevated temperatures and improve its superplastic behaviour [37].

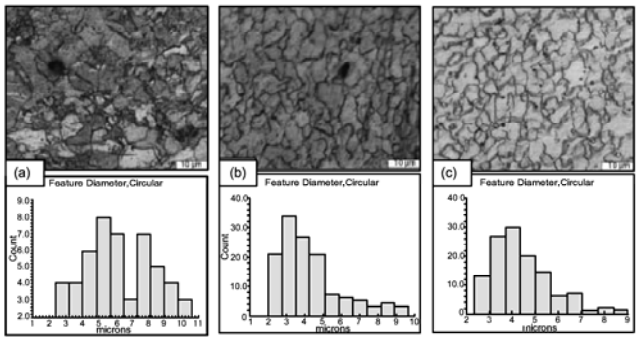

Figure 18. Microstructure of (a) as-received, (b) FS processed sample at 1200 rpm and 22 in/min, and (c) FS processed sample at 1200 rpm and 25 in/min [37]

Thermocouple data from plasticine weld experiments, along with predicted temperatures from each boundary condition, are shown in Fig. 19. The thermocouple measurements reveal the maximum temperature experienced by the thermocouple during welding, which may occur slightly upstream or downstream of the pin. Generally, the experimental data and the variable shear stress model are in good agreement. Both constant velocity models with α= 0.1 and 1.0 predict conditions which are hotter than the measured values. For α = 0.01 the predicted temperatures at the retreating side are nearly identical to the measured values. However, temperatures at the advancing side are underestimated and the variable shear stress model is more accurate for this aspect of the problem.

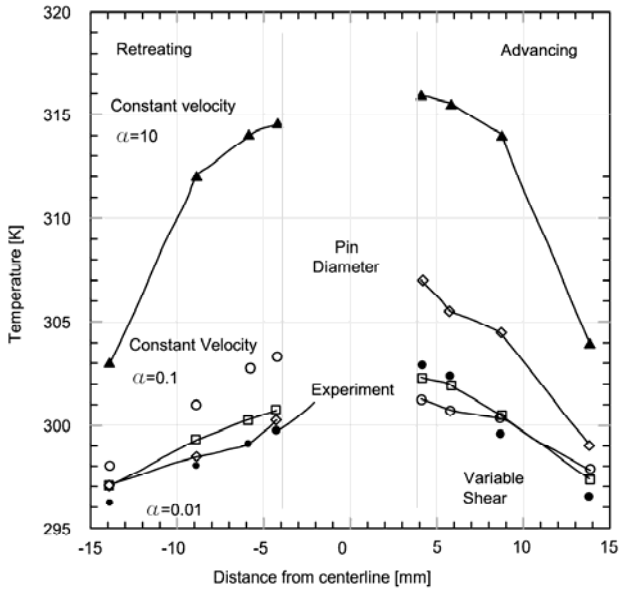

Figure 19. Peak temperatures near the pin during plasticine FSW [38]. α = relative velocity of the material adjacent to the rotating tool and is assumed to be equal to some fraction of tool velocity

Mishra and Ma, 2005 [39] friction stir welded a 6.35 mm thick 7075Al-T651 plate and measured the temperature distribution around the stirred zone, both as a function of distance from the stirred zone and through the thickness of the sheet. Figure 20 shows the peak temperature distribution adjacent to the stirred zone. Figure 20 reveals three important features. First, maximum temperature was recorded at locations close to the stirred zone, i.e., the edge of the stirred zone, and temperature decreased with increasing distance from the stirred zone. Second, the temperature at the edge of the stirred zone increased from the bottom surface of the plate to the top surface. Third, a maximum temperature of 475°C was recorded near the corner between the edge of the stirred zone and the top surface. This temperature is believed to exceed the solution temperature for the hardening precipitates in 7075Al-T651. Based on these results the temperature within the stirred zone is surmised to be above 475°C. However, the maximum temperature within the stirred zone was less than the melting point of 7075Al because no evidence for material melting was observed in the weld.

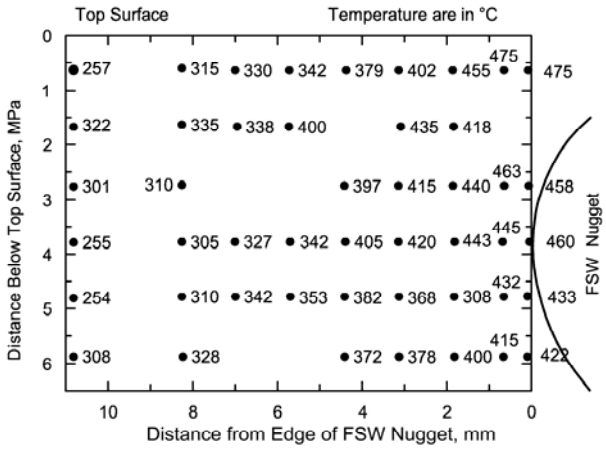

Figure 20. Peak temperature distribution adjacent to a friction stir weld in 7075Al-T651. The line on the right side of figure shows the nugget boundary [39]

Concluding Remarks

The foregoing review of SPD and FSP/ FSW clearly reveals that in these two fields, as indeed in many others, experiments are way ahead of theory. In our opinion, it is essential to answer at least the following questions if these techniques are to graduate from their present status of evolving creative arts to well-grounded technologies over which a rigorous control can be exercised during processing.

1. What is/ are the values of the friction coefficient(s) in friction stir processing? Various models assume a constant value, but the framework and justification is missing. This leads to uncertainty in thermal and material flow modeling. Could there also be cases of sticking friction or a mixture of sliding and sticking friction?
2. In predictive modeling of the thermal input during the friction stir process, what are the various components of the heat input? This question should also include a discussion on the critical evaluation of the various experimental verification techniques.
3. In both the processes how to determine the strain and strain rate accurately? Or, should these be defined in terms of a range? The discussion should also include a

critical evaluation of the various models and estimate methods.

4. Again in both the methods, how does the material flow depend on the process parameters and tool design? Experimental evidence suggests that under certain conditions and tool pin geometry in FSP/ FSW, the material does go around the pin more than once. The discussion in both cases should lead to a framework for various material flow observations, including the onion ring pattern in FSP/ FSW.
5. What is the overall model for microstructural evolution at large strain at high strain rate? Discussion should include mechanisms that lead to nucleation of nanocrystalline grains next to the pin in FSP/ FSW and microstructural evolution of processed material under the shoulder at the trailing side of the tool. How do the material chemistry and overall heat input influence microstructure evolution? Discussion should include not only the differences in experimental observations among various alloys, but also various metallic systems. For example, differences in microstructure development in aluminum and titanium alloys.
6. How do changes in material flow and thermal input lead to different types of defect formation?
7. What are the key features of the friction stirred microstructures that influence the resultant properties? Are there some unique features in friction stirred microstructures because of superimposed deformation and thermal cycles?

In our view, analyses of both the problems of SPD and FSP/ FSW are formidable and industrially relevant solutions can be evolved only by a systems approach involving materials – design – mechanics and product formation. As a practical alternative, an approach based on neural networks may be adopted.

Acknowledgment

This paper is written while KAP is the Mercator Visiting Professor at University of Muenster. He thanks the DFG for the grant of this position.

References

1. K.J. Kurzydlowski, H. Garbacz and M. Richert, *Rev. Adv. Mater. Sci*., 8 (2004)129-133.
2. J. Zrnik, T. Kovarik, Z. Novy, M. Cieslar, *Materials Science and Engineering: A*, 503 (2009) 126-129.
3. V.M. Segal, Patent No. 575892, 1977.
4. R.Z Valiev, R.R Mulyukov, V.V Ovchinnikov, *Philos. Mag. Lett.*, 1990; 62:253.
5. Y. Saito, N. Tsuji, H. Utsonomiya, T. Sakai, R.G. Hong, *Scr. Mater.,* 39 (1998) 1221.
6. A.K. Gosh, *U.S. Patent 4,721,537*, January 26, 1988.
7. Y.T. Zhu, T.C. Lowe, H. Jiang, J. Huang, *U.S. Patent.6197129 B1*, 2001.
8. H. Petryk, S. Stupkiewicz, *Materials Science and Engineering A*, 444 (2007) 214–219.
9. M. Kai, Z. Horita, T.G. Langdon, *Materials Science and Engineering A*, 488(2008) 117-124.
10. M.A. Munoz Morris, I. Gutierrez-Urrutia, D.G. Morris, *Materials Science and Engineering: A*, 493, (1-2) (2008) 141-147.
11. S. Li , A.A. Gazder, I.J. Beyerlein, C.H.J. Davies, E.V. Pereloma, *Acta Materialia,* 55 (2007) 1017–1032.
12. T.G. Langdon, *Materials Science and Engineering: A,* 462 (2007) 3–11.
13. K.A. Padmanabhan, R.A. Vasin and F.U. Enikeev, *Super plastic Flow: Phenomenology and Mechanics*, Springer Verlag, Berlin-Heidelberg-New York, March 2001.
14. H.S. Kim, M.H. Seo, S.I. Hong, *Materials Science and Engineering: A*, 291 (2000) 86–90.
15. R.Z. Valiev, T.G. Langdon, *Progress in Materials Science*, 51(2006)881-981.
16. I. Gutierrez-Urrutia, M.A. Munoz-Morris, I. Puertas, C. Luis, D.G. Morris, *Materials Science and Engineering: A,* 475 (2008) 268–278.
17. H.S. Kim, M.H. Seo, S.I. Hong, *Journal of Materials Processing Technology*, 130–131 (2002) 497–503.
18. C.J. Luis Perez, *Scripta Materialia,* 50 (2004) 387–393.
19. I. Gutierrez-Urrutia, M.A. Muñoz-Morris, D.G. Morris, *Acta Materialia*, 55 (2007)1319-1330.
20. S.H. Kang, Y.S. Lee, J.H. Lee, *Journal of Materials Processing Technology*, 201(2008) 436-440.
21. P.B. Prangnell, J.R. Bowen, P.J. Apps, *Materials Science and Engineering A*, 375-377 (2004) 178-185.
22. K. Sitarama Raju, M. Ghanashyam Krishna, K.A. Padmanabhan, K. Muraleedharan, N.P. Gurao, G. Wilde, *Materials Science and Engineering: A*, 491(2008) 1-7.
23. G. Sakai, Z. Horita, T.G. Langdon, *Materials Science and Engineering A*, 393(1-2)(2005)344-351.
24. A.P. Zhilyaev, K. Oh-Ishi, T.G. Langdon, T.R. McNelley, *Materials Science and Engineering: A*, 410-411, (2005) 277-280.
25. M. Kai, Z. Horita, T.G. Langdon, *Materials Science and Engineering: A*, 488, (1-2) (2008)117-124.
26. Z. Horita, T.G. Langdon, *Materials Science and Engineering A*, 410–411 (2005) 422–425.
27. G. Sakai, K. Nakamura, Z. Horita, T.G. Langdon, *Materials Science and Engineering: A*, 406(1-2) (2005)268-273.
28. A. P. Zhilyaev, S. Lee, G.V. Nurislamova, R.Z. Valiev, T.G. Langdon, *Scripta Materialia*, 44(2001) 2753-2758.
29. T. Hebesberger, H.P. Stüwe, A. Vorhauer, F. Wetscher, R. Pippan, *Acta Materialia*, 53, 2(2005)393-402.
30. I. Charit, R.S. Mishra, *Scripta Materialia,* 58 (2008) 367–371.
31. K. Elangovan, V. Balasubramanian, *Materials and Design*, 29 (2008) 362–373.
32. R. S. Mishra, *Scripta Materialia,* 58 (2008) 325–326.
33. Z.Y. Ma, R.S. Mishra, M.W. Mahoney, R. Grimes, *Materials Science and Engineering A*, 351 (2003) 148-153.
34. I. Charit, R.S. Mishra, *Scripta Materialia*, 58 (2008) 367-371.
35. Z.Y. Ma, R.S. Mishra, M.W. Mahoney, *Scripta Materialia*, 50 (2004) 931–935.
36. L. Commin, M. Dumont, J.-E. Masse, L. Barrallier **,** *Acta Materialia*, 57 (2009)326-334.
37. B.M. Darras, M.K. Khraisheh, F.K. Abu-Farha, M.A. Omar, *Journal of Materials Processing Technology*, 191 (2007) 77-81.
38. B.C. Liechty, B.W. Webb, International Journal of Machine Tools & Manufacture, 48 (2008) 1474– 1485.
39. R.S. Mishra, Z.Y. Ma, Materials Science and Engineering R 50 (2005) 1–78.